

# Multivariable Control Designs for Piezoelectric tubes

B. Bhikkaji\*

Y. K. Yong, I. A. Mahmood, S. O. R. Moheimani\*\*

\* *Indian Institute of Technology Madras, Chennai, India  
(e-mail: Bharath.Bhikkaji@iitm.ac.in).*

\*\* *University of Newcastle, NSW, Australia,  
(e-mail: YuenKuan.Yong@newcastle.edu.au,  
Iskandar.Mahmood@newcastle.edu.au and  
Reza.Moheimani@newcastle.edu.au)*

---

**Abstract:** Most AFMs use piezoelectric tube nanopositioners for scanning. Fast actuation of piezoelectric tubes are restricted due to the presence of low mechanical resonant modes. These resonances, when excited, set off vibrations that cause loss of precision and repeatability of the scans. Thereby restricting the scanning frequencies to less than 1% of the first resonance frequency. Here, an innovative multivariable control design methodology for damping the resonant modes of the tube is presented. This methodology exploits the symmetry present in transfer-functions relating the input and output, and converts the multivariable control design problem into independent SISO designs. This methodology in conjunction with Integral Resonant control is used for damping the first resonant mode of the tube, and enables scans upto 10% of the first resonant mode. The proposed methodology can be applied to a large class of parallel kinematics nanopositioners used in scanning probe microscopes and probe-based data storage systems.

*Keywords:* Atomic Force Microscopes, Piezoelectric tubes, Nanopositioners, Resonance, Multivariable Control and Integral Resonant Control.

---

## 1. INTRODUCTION

Atomic Force Microscopes (AFMs) were invented in the mid 80's, G. Binnig, C. F. Quate and C. Gerber (1986), for generating topographical maps of solid surfaces at micro to atomic resolution.

In an AFM, a cantilever with a sharp probe (of few atomic dimensions in width) is placed in contact with the material sample for which a topographical map is desired. A laser source is focused on the probe end of the cantilever, and the reflection from the cantilever is captured by a Photo Sensitive Diode (PSD), see Figure 1. The given sample is scanned by moving it in a raster pattern, which causes the cantilever to deflect due to variations in the sample topography. These deflections vary the intensity of light captured by the PSD, which, in turn, is used for generating the topography of the surface. In many commercial microscopes samples are scanned by placing them on a piezoelectric tube and actuating it in a raster pattern.

When actuating the piezoelectric tube in a raster pattern, the tube tracks a triangular waveform along the  $x$ -axis and a slowly increasing ramp, or a slowly increasing staircase function, along the  $y$ -axis. The fundamental frequency of the triangular waveform is referred to as the scanning rate. Actuation of piezoelectric tubes are hampered by the presence of low mechanical resonances. Higher scanning rates excite the resonance, inducing mechanical vibrations.

Typically, to avoid vibrations, the scanning rates are restricted to 1% of the resonance frequency, Fleming et al. (2008).

A standard paradigm for the actuation of a piezoelectric tube has been to design a feedback controller that would damp the resonance along the  $x$  axis, Bhikkaji et al. (2007). This would enable the tube to track triangular waveforms with higher fundamental frequencies than 1% of the resonance frequency (or achieve higher scanning rates). The actuation along the  $y$  axis is done in open loop, as the tracking signal therein is either a slowly varying ramp or a stair case function. However, this would not completely eliminate vibrations, as there would be cross coupling between the  $x$  and  $y$  axis. A more comprehensive paradigm would be to design a multivariable controller that would damp resonances of all the transfer-functions involved. Though this has been attempted before, the design methodologies followed have been simplistic (by ignoring the cross coupling and assuming the dynamics along the  $x$  and  $y$  axis to be independent), A. Daniele, S. Salapaka, M. V. Salapaka and M. Dahleh (1999); Schitter et al. (2003). This paper presents an elegant method for designing a multivariable controller for piezoelectric tubes. Unlike the above mentioned papers, here the presence of cross coupling between the axes are not neglected.

Due to symmetry, the dynamic response of piezoelectric tubes to inputs along  $x$  and  $y$  axis are similar. This allows for the decoupling of the tube dynamics. A multi-variable

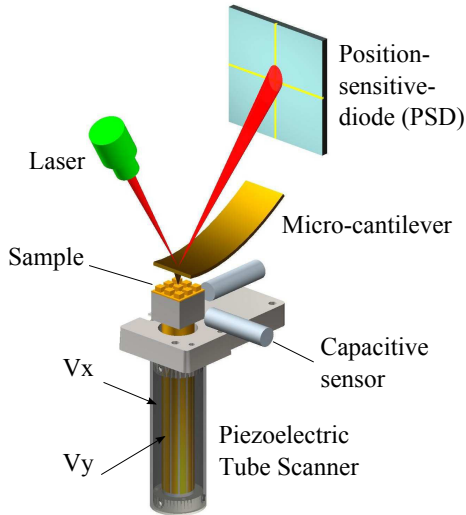


Fig. 1. Schematic of an AFM

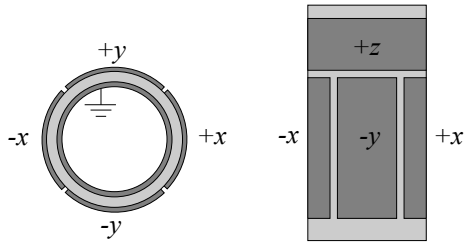


Fig. 2. Schematics of the piezoelectric tube scanner

controller with a similar structure enables the conversion of MIMO control design into independent SISO designs. Here, a multivariable Integral Resonant controller bearing the same structure as the plant is designed to achieve good damping of the resonances. The design procedure presented here is simple, tractable and very efficient.

## 2. EXPERIMENTAL SETUP

The piezoelectric tube scanner considered here is a thin walled cylindrical tube made of a piezoelectric material. The inner and outer layers of the tube are coated with a layer of silver. The external electrode of the tube scanner is quartered into four equal sections, see Figure 2 for an illustration. It also has a small continuous electrode at the top of the tube for  $z$ -axis actuation. The inner continuous electrode is always grounded. One end of the tube scanner is fixed to a base. An aluminum cube is glued to the free end of the tube, this serves as a stage over which a sample is placed. In Figure 2,  $x+$  and  $y+$  are the actuation points, while  $x-$  and  $y-$  denote the sensing points. When voltage signals  $v_{x+}$  and  $v_{y+}$  are applied at  $x+$  and  $y+$ , respectively, the piezoelectric tube deforms inducing voltages  $v_{x-}$  and  $v_{y-}$  at  $x-$  and  $y-$ , respectively. These voltages are recorded as outputs. For  $z$ -axis actuation, a voltage is applied to the continuous  $z$ -electrode.

An NT-MDT NTEGRA scanning probe microscope (SPM) is used for performing experiments. This SPM is capable of performing scans in air and liquid. The SPM software limits the image resolution relative to scanning speed. At the highest resolution,  $256 \times 256$  scan lines, the fastest

achievable scanning frequency is limited to 31 Hz. The SPM is configured to operate as an AFM. The piezoelectric tube scanner of the SPM is replaced by the above mentioned tube scanner. The  $x+$  and  $y+$  axes of the tube are driven by a NANONIS bipolar high voltage amplifier HVA4. This amplifier has a maximum gain of 40 and a voltage range of 400 V. Two ADE Technologies 8810 capacitive sensors were placed in close proximity to the adjacent surfaces of the sample holder (aluminum cube) to observe the displacements of the tube along the  $x$  and  $y$  axes see Figure 1. The AFM controller was used to generate the  $x+$  and  $y+$  signals. These were accessed through the AFM signal access module and were applied to the controlled piezoelectric tube scanner through the high voltage amplifiers. A dSPACE-1103 rapid prototyping system was used to implement the  $x$  and  $y$  axes feedback controllers in real-time. The  $z$ -axis displacement was controlled using the AFM software and circuitry.

The nanopositioning system is interpreted as having two linear subsystems

$$Y_v(s) = G_v(s)U(s) \quad (1)$$

and

$$Y_d(s) = G_d(s)U(s) \quad (2)$$

where  $Y_v(s)$  is the Laplace transform of  $[v_{x-}, v_{y-}]^T$ , voltages induced at the sensing patches  $x-$  and  $y-$ ,  $Y_d(s)$  is the Laplace transform of  $[d_x, d_y]^T$ , displacement measurements of the capacitive sensors along  $x$  and  $y$  directions,  $U(s)$  is the Laplace transform of  $[v_{x+}, v_{y+}]^T$ , voltage signals applied at the  $x+$  and  $y+$  electrodes,

$$G_v(s) = \begin{bmatrix} G_{xx}(s) & G_{xy}(s) \\ G_{yx}(s) & G_{yy}(s) \end{bmatrix} \quad (3)$$

and

$$G_d(s) = \begin{bmatrix} G_{d_{xx}}(s) & G_{d_{xy}}(s) \\ G_{d_{yx}}(s) & G_{d_{yy}}(s) \end{bmatrix}, \quad (4)$$

transfer-functions relating the inputs  $[v_{x+}, v_{y+}]^T$  and the outputs  $[v_{x-}, v_{y-}]^T$  and  $[d_x, d_y]^T$  respectively.

## 3. SYSTEM IDENTIFICATION

Swept sine waves  $v_{x+}$  and  $v_{y+}$ , within the frequency range of 10 Hz to 10 kHz, are applied at the  $x+$  and  $y+$  electrode respectively. The corresponding voltages  $v_{x-}$  and  $v_{y-}$  induced at  $x-$  and  $y-$  electrodes are recorded. The frequency response functions (FRF) relating the inputs  $[v_{x+}, v_{y+}]^T$  and the recorded outputs  $[v_{x-}, v_{y-}]^T$  are plotted in Figures 3 and 4. The displacements  $d_x$  and  $d_y$  measured by the capacitive sensors are also recorded and the FRFs relating them to the input  $[v_{x+}, v_{y+}]^T$  are plotted in Figures 5 and 6.

Here, subsystem (1) will be used for control design while the capacitive sensor responses, *i.e.*, subsystem (2), will be used for monitoring the displacements along  $x$  and  $y$  axes. Therefore, only transfer-functions of the matrix  $G_v(s)$ , (1), are modeled.

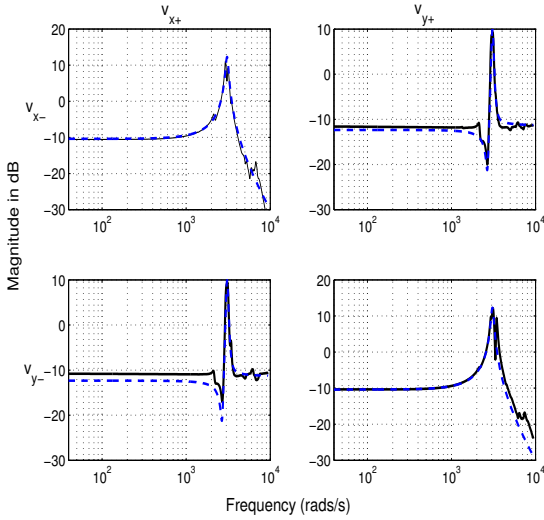


Fig. 3. Magnitude of the Frequency response functions (FRFs) relating the inputs  $[v_{x+}, v_{y+}]^T$  and the outputs  $[v_{x-}, v_{y-}]^T$ . Dashed plots (---) denote the magnitude response of the models estimated, while the continuous (-) plots denote the experimentally determined magnitude response.

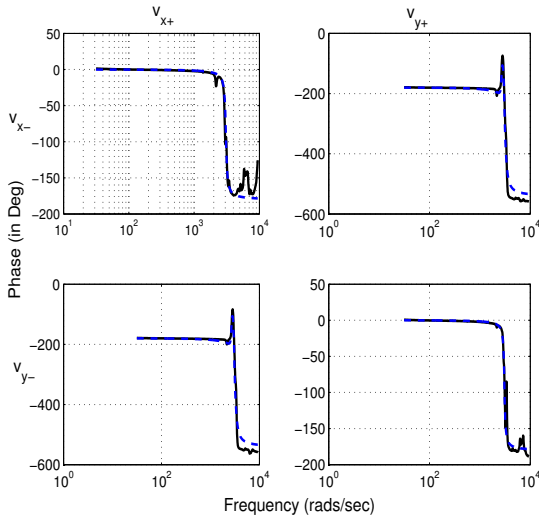


Fig. 4. Phase of the Frequency response functions (FRFs) relating the inputs  $[v_{x+}, v_{y+}]^T$  and the outputs  $[v_{x-}, v_{y-}]^T$ . Dashed plots (---) denote the phase response of the models estimated, while the continuous (-) plots denote the experimentally determined phase response.

Since the tube is symmetrically segmented one would expect that  $G_{xx}(j\omega) = G_{yy}(j\omega)$  and  $G_{xy}(j\omega) = G_{yx}(j\omega)$ . However, invariably due to errors introduced when manufacturing tube (like the tube being not uniformly thick or not having a constant density), unsymmetrical gluing of the aluminum cube and uneven fastening of to the tube to the base, they can be only approximately equal. This is evident from Figure 3. Nevertheless for control design, it is assumed that  $G_{xx}(j\omega) = G_{yy}(j\omega)$  and  $G_{xy}(j\omega) = G_{yx}(j\omega)$ .

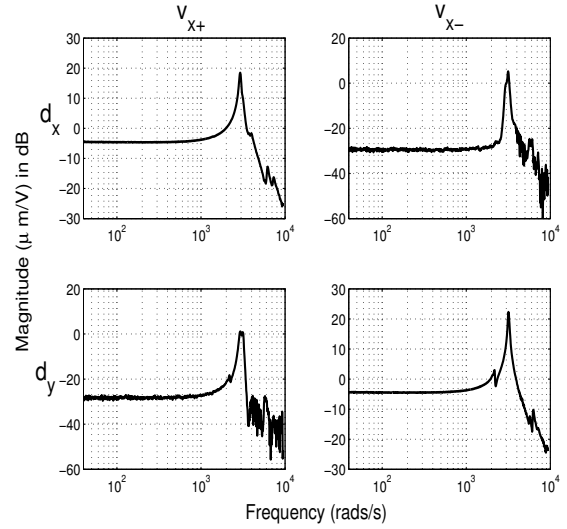


Fig. 5. Magnitude of the Frequency response functions (FRFs) relating the he inputs  $[v_{x+}, v_{y+}]^T$  and the Capacitive sensor outputs  $[d_x, d_y]^T$ .

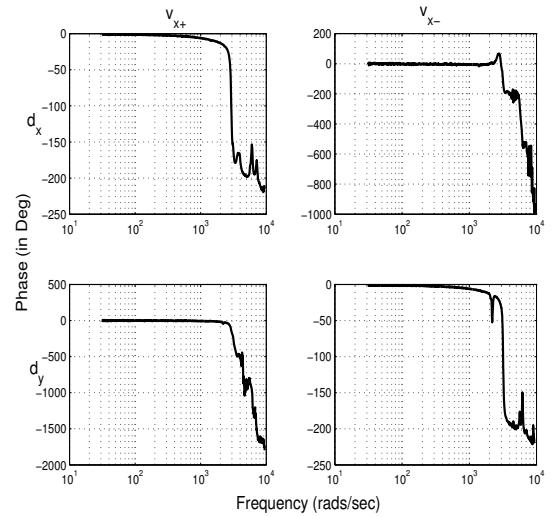


Fig. 6. Phase of the Frequency response functions (FRFs) relating the he inputs  $[v_{x+}, v_{y+}]^T$  and the Capacitive sensor outputs  $[d_x, d_y]^T$ .

The following models have been fit for the FRF data plotted in Figure 3,

$$G_1(s) = \frac{2.851e006}{s^2 + 225s + 9.432e006} \quad (5)$$

and

$$G_2(s) = \frac{-0.27(s^2 + 160s + 7.2e06)}{(s^2 + 225s + 9.432e06)} \times \frac{(s^2 - 600s + 1.1e07)}{(s^2 + 225s + 9.432e06)}, \quad (6)$$

where  $G_1(s) = G_{xx}(s) = G_{yy}(s)$  and  $G_2(s) = G_{xy}(s) = G_{yx}(s)$ .

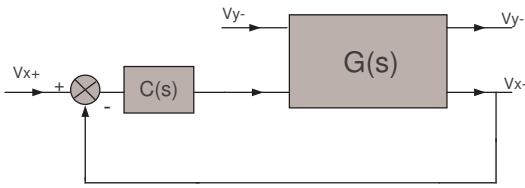


Fig. 7. Standard control paradigm followed for actuation of piezoelectric tubes.

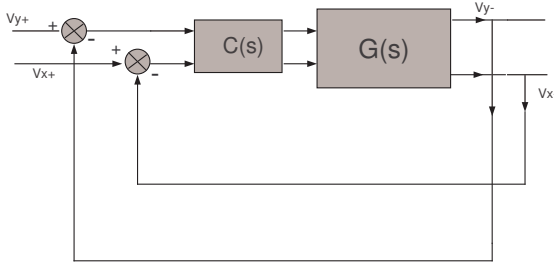


Fig. 8. Multivariable control of the piezoelectric tube.

#### 4. CONTROL METHODOLOGY

The standard paradigm for control of piezoelectric tubes has been to damp the resonance along the  $x$  axis. That is to damp the resonance of  $G_{xx}(s)$ , using a feedback controller, and to actuate the tube in a raster pattern, see Figure 7. This, however, does not completely eliminate vibrations, as the resonance along the  $y$  axis is not damped.

In order to damp resonances along both the axes a multivariable controller, Figure 8, that regulates both inputs have to be designed. In Mahmood and Moheimani (2009); A. Daniele, S. Salapaka, M. V. Salapaka and M. Daleh (1999); Schitter et al. (2003) the authors have ignored cross coupling, *i.e.*, have set  $G_{xy}(s) = G_{yx}(s) = 0$  in (3), and designed controllers of the form

$$C(s) = \begin{bmatrix} C_{xx}(s) & 0 \\ 0 & C_{yy}(s) \end{bmatrix} \quad (7)$$

to damp resonances along both the axes. This could result in closed-loop instabilities. For example, it can be checked that (7), with

$$C_{xx}(s) = C_{yy}(s) = \frac{-10000}{s + 5000} \quad (8)$$

will stabilize  $G_v(s)$ , (3), when  $G_1(s) = G_{xx}(s) = G_{yy}(s)$ , and  $G_{xy}(s) = G_{yx}(s) = 0$ . But, it will not stabilize  $G_v(s)$  with  $G_{xy}(s) = G_{yx}(s) = G_2(s)$ .

To the best of authors knowledge fully multivariable controllers of the form

$$C(s) = \begin{bmatrix} C_{xx}(s) & C_{xy}(s) \\ C_{yx}(s) & C_{yy}(s) \end{bmatrix} \quad (9)$$

are rarely designed.

Note that

$$\begin{aligned} G_v(s) &= \begin{bmatrix} G_{xx}(s) & G_{xy}(s) \\ G_{yx}(s) & G_{yy}(s) \end{bmatrix} \\ &= \begin{bmatrix} G_1(s) & G_2(s) \\ G_2(s) & G_1(s) \end{bmatrix} \\ &= M^T \begin{bmatrix} G_+(s) & 0 \\ 0 & G_-(s) \end{bmatrix} M, \end{aligned} \quad (10)$$

where

$$M = M^T = \frac{1}{\sqrt{2}} \begin{bmatrix} 1 & 1 \\ 1 & -1 \end{bmatrix}, \quad (11)$$

$$G_+(s) = G_1(s) + G_2(s) \quad (12)$$

and

$$G_-(s) = G_1(s) - G_2(s). \quad (13)$$

Similarly, in  $C(s)$ , (9), if  $C_1(s) = C_{xx}(s) = C_{yy}(s)$  and  $C_2(s) = C_{xy}(s) = C_{yx}(s)$  then

$$C(s) = M^T \begin{bmatrix} C_+(s) & 0 \\ 0 & C_-(s) \end{bmatrix} M, \quad (14)$$

where

$$C_+(s) = C_1(s) + C_2(s) \quad (15)$$

and

$$C_-(s) = C_1(s) - C_2(s). \quad (16)$$

This implies that Loop transfer-function of Figure 8 is

$$\begin{aligned} L(s) &= G_v(s)C(s) \\ &= M^T \begin{bmatrix} C_+(s)G_+(s) & 0 \\ 0 & C_-(s)G_-(s) \end{bmatrix} M. \end{aligned} \quad (17)$$

Hence the closed loop poles are zeros of

$$\begin{aligned} I + L(s) &= I + G_v(s)C(s) \\ &= M^T \begin{bmatrix} 1 + C_+(s)G_+(s) & 0 \\ 0 & 1 + C_-(s)G_-(s) \end{bmatrix} M, \end{aligned} \quad (18)$$

where  $I$  is the  $2 \times 2$  identity matrix. This in turn implies that the closed loop poles are zeros of

$$1 + C_+(s)G_+(s) = 0 \quad (19)$$

and

$$1 + C_-(s)G_-(s) = 0. \quad (20)$$

Thus designing a multivariable controller now boils down to designing controllers  $C_+(s)$  and  $C_-(s)$  for scalar transfer-functions  $G_+(s)$  and  $G_-(s)$  respectively. Designing controllers for SISO plants are mathematically tractable and their stability properties can be easily analyzed using root-locus plots. Here, Integral resonant control (IRC), described by Aphale et al. (2007), is used for designing controllers  $C_+(s)$  and  $C_-(s)$ , as they are known to give good performance and possess a simple model structure.

## 5. EXPERIMENTAL RESULTS

Design of IRC using root locus is discussed in detail in Aphale et al. (2007) and Bhikka,ji and Moheimani (2008). Here, it suffices to say that we have chosen

$$C_+(s) = C_-(s) = \frac{-10^4}{s + 8000}. \quad (21)$$

The choice was made, using the root-locus procedure outlined in the above mentioned references, such that the closed-loop system is sufficiently damped.

In Figure 9, open loop data, presented in Figures 3 and 4, is plotted along with the simulated closed loop model. Simulations predict a 20dB damping. As done in Section 3, swept sine waves, within the frequency range of 10 Hz to 10 kHz, are applied at the  $x+$  and  $y+$  electrodes, and the corresponding voltages induced at the  $x-$  and  $y-$  electrodes are measured in closed loop. The closed loop FRFs relating the inputs applied at  $x+$  and  $y+$  electrodes and outputs recorded at  $x-$  and  $y-$  electrodes are plotted in Figure 9. It can be observed from the plots that simulations closely match the experimental results. A similar damping can be observed in the closed loop FRFs relating the inputs and the capacitive sensor outputs plotted in Figure 10.

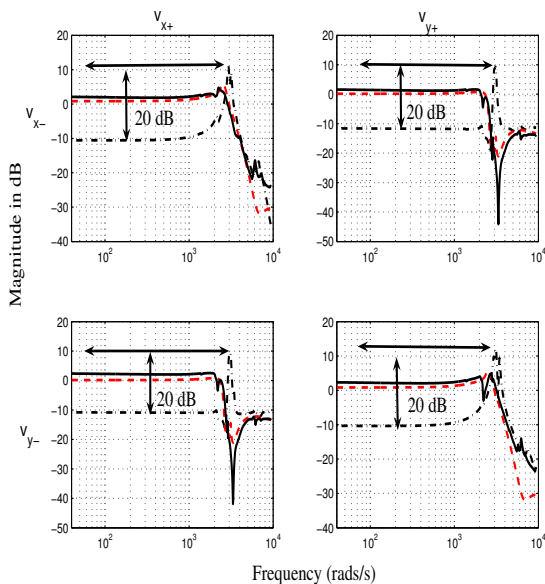


Fig. 9. Magnitude response of the closed loop FRFs relating the inputs  $[v_{x+}, v_{y+}]^T$  and the outputs  $[v_{x-}, v_{y-}]^T$ . Dashed plots (- -) denote simulated closed loop FRFs, dashed dots (-.) denotes open loop FRFs and continuous (-) plots denotes experimentally determined closed loop FRFs.

## 6. AFM IMAGES

In this section, scan images of a calibration grating are obtained to evaluate the performance of the damping controller. A MikroMasch TZG2 calibration grating which has parallel rectangular features, with 3  $\mu\text{m}$  period and 108nm height, was used for experiments. A contact mode

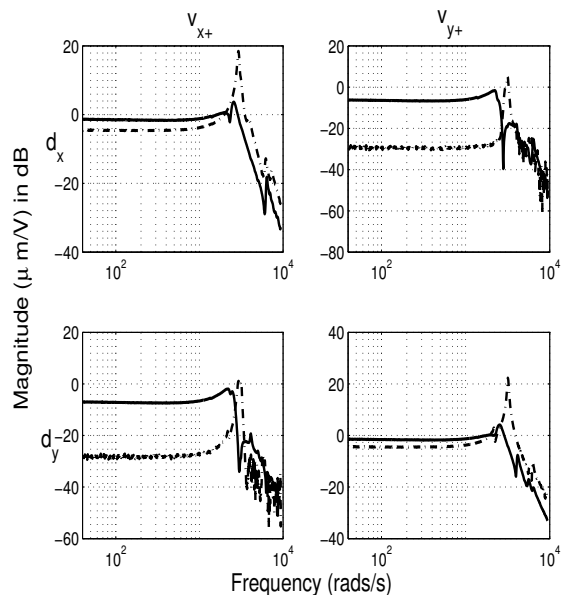


Fig. 10. Magnitude response of the closed loop FRFs relating the inputs  $[v_{x+}, v_{y+}]^T$  and the outputs  $[d_x, d_y]^T$ . Dashed plot (- -) denotes open loop FRFs and continuous (-) plots denote experimentally determined closed loop FRFs.

cantilever with a resonance frequency of 13kHz was used to perform scans. The first dominant mode of the  $x$  and  $y$  axes was suppressed in closed-loop using the Integral Resonant control technique presented in Sec. 4.  $4\mu\text{m} \times 4\mu\text{m}$  open- and closed-loop images with  $256 \times 256$  lines of the grating were obtained in constant height contact mode at 5Hz, 10Hz, 15.6Hz and 31.25Hz.

Figs. 11 and 12 show the open- and closed-loop images (with activated IRC) respectively. Oscillations are visible in all open-loop scans which distort the images severely, in particular at 31.25Hz. Oscillations are also observed in time signals. With the IRC activated, oscillations are eliminated in all four scan frequencies.

## 7. CONCLUSION

Atomic Force microscopes (AFM) use piezoelectric tubes for nanopositioning. Piezoelectric tubes possess lightly damped resonant modes that cause mechanical vibrations. Thereby, restricting the scanning rates to less than 1% of the first resonance frequency. In this paper a symmetrically quartered piezoelectric tube, typically used in AFMs as nanopositioner, was considered. In order to actuate this tube in a raster pattern, resonant modes along both  $x$  and  $y$  axes have to be damped. It was noted control designs that neglect the cross coupling in the tube dynamics could cause closed loop instability. As the tube is symmetrically quartered the transfer-function matrix relating the voltages applied at the  $x+$  and  $y+$  electrodes and the voltages induced at the  $x-$  and  $y-$  electrodes is symmetric. A controller with a similar structure as the plant was found to convert the MIMO control design problem into independent SISO designs. IRC controllers were designed for the individual SISO plants. A 20 dB damping was achieved along both the  $x$  and  $y$  axes. Scan images were recorded in open- and closed-loop at 5Hz,

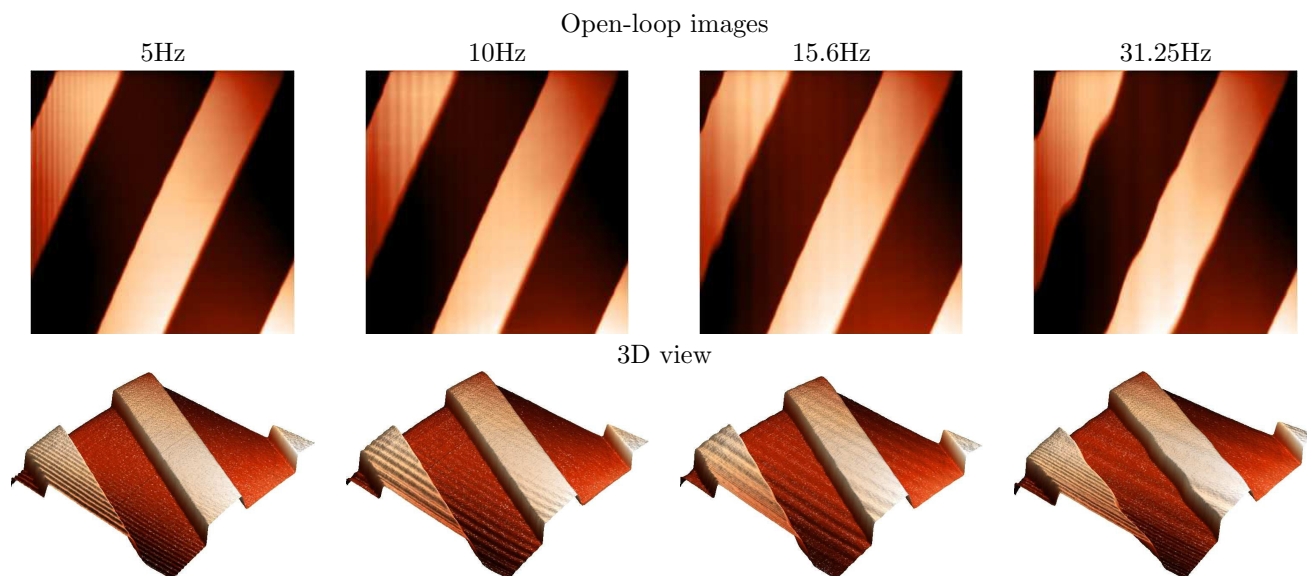


Fig. 11. Open-loop images ( $256 \times 256$  scan lines) of a  $4\mu\text{m} \times 4\mu\text{m}$  scan area.

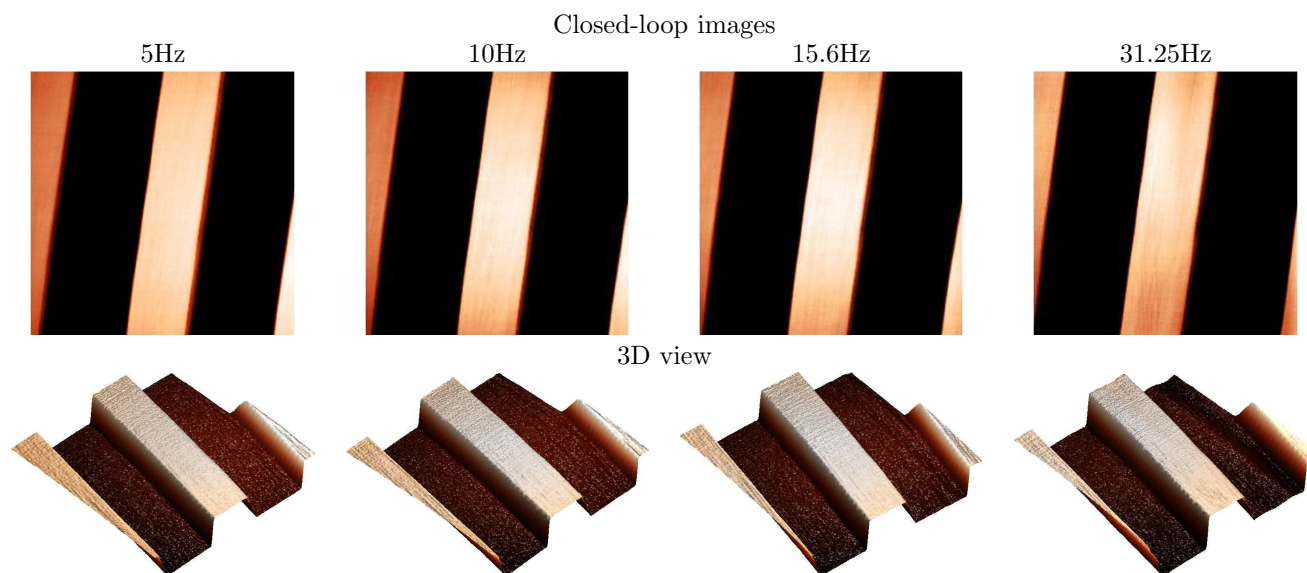


Fig. 12. Closed-loop images ( $256 \times 256$  scan lines) of a  $4\mu\text{m} \times 4\mu\text{m}$  scan area.

10Hz, 15.6 Hz and 31.5Hz. With the damping controller activated, oscillations in the scan images were eliminated which improve the image quality substantially.

#### REFERENCES

- A. Daniele, S. Salapaka, M. V. Salapaka and M. Daleh (1999). Piezoelectric Tubes for Atomic Force Microscopes: Design of Lateral Sensors, Identification and Control. *in Proc. of the ACC, San Diego, California*, 253–257.
- Aphale, S., Fleming, A.J., and Moheimani, S.O.R. (2007). Integral resonant control of collocated smart structures. *Smart Materials and Structures*, 16(2), 439–446.
- Bhikkaji, B. and Moheimani, S.O.R. (2008). Integral resonant control of a piezoelectric tube actuator for fast nano-scale positioning. *IEEE/ASME Transactions on Mechatronics*, 13(5), 530–537.
- Bhikkaji, B., Ratnam, M., Fleming, A.J., and Moheimani, S.O.R. (2007). High-performance control of piezoelectric tube scanners. *IEEE Transactions on Control Systems Technology*, 5(5), 853–866.
- Fleming, A.J., Wills, A., and Moheimani, S.O.R. (2008). Sensor fusion for improved control of piezoelectric tube scanners. *IEEE Transactions on Control Systems Technology*, 16(6), 1265–1276.
- G. Binnig, C. F. Quate and C. Gerber (1986). Atomic force microscopes. *Phys Rev Lett*, 56(9), 930–933.
- Mahmood, I.A. and Moheimani, S.O.R. (2009). Making a commercial afm more accurate and faster using positive position feedback control. *Review of Scientific Instruments*, 80(6). Article No.: 063705.
- Schitter, G., Stemmer, A., and Allgower, F. (2003). Robust 2dof-control of a piezoelectric tube scanner for high speed atomic force microscopy. *Proceedings of the American Control Conference*, 5, 3720 – 3725.